Published in final edited form as:
Bone. 2011 June 1; 48(6): 1291–1297. doi:10.1016/j.bone.2011.03.755.

Quantitative characterization of subject motion in HR-pQCT images of the distal radius and tibia

Miki Sode[1,2], **Andrew J. Burghardt**[2], **Jean-Baptiste Pialat**[2,3,4], **Thomas M. Link**[2], and **Sharmila Majumdar**[1,2]

[1] Joint Graduate Group in Bioengineering, University of California at San Francisco and Berkeley, San Francisco and Berkeley, California, USA

[2] Musculoskeletal Quantitative Imaging Research Group, Department of Radiology and Biomedical Imaging, University of California at San Francisco, San Francisco, California, USA

[3] INSERM U831 and Université de Lyon, Lyon, France

[4] Edouard Herriot Teaching Hospital, Hospices Civils de Lyon, Lyon, France

Abstract

Image quality degradation due to subject motion is a common artifact affecting *in vivo* high-resolution peripheral quantitative computed tomography (HR-pQCT) of bone. These artifacts confound the accuracy and reproducibility of bone density, geometry, and cortical and trabecular structure measurements. Observer-based systems for grading image quality and criteria for deciding when to repeat an acquisition and post hoc data quality control remain highly subjective and non-standardized. This study proposed an objective, quantitative technique for measuring subject motion in HR-pQCT acquisitions from the raw projection data, using image similarity measures applied to the parallelized projections at 0° and 180°.

A total of 88 HR-pQCT exams with repeated acquisitions of the distal radius (N=54) or distal tibia (N=34) of 49 women (age = 59 ± 14 yr) and 3 men (46 ± 2 yr) were retrospectively evaluated. All images were graded from 1 (no visible motion artifacts) to 5 (severe motion artifacts) according to the manufacturer-suggested image quality grading system. In addition, to serve as the reference case without motion artifacts, two cadaveric wrists and two ankles specimens were imaged twice with repositioning. The motion-induced error was calculated as the percent difference in each bone parameter for the paired scans with and without visually apparent motion artifacts. Quantitative motion estimates (QMEs) for each motion-degraded scan were calculated using two different image similarity measures: sum of squared differences (SSD) and normalized cross-correlation (NCC).

The mean values of QME_{SSD} and QME_{NCC} increased with the image quality grade for both radius and tibia. The quality grades were differentiated between grade 2 and 3 using QME_{SSD}, but not with QME_{NCC}, in addition to between grade 4 and 5. Both QMEs correlated significantly to the motion-induced errors in the measurements and their empirical relationship was derived. Subject

Corresponding Author: Miki Sode, Ph.D., Musculoskeletal Quantitative Imaging Research Group, QB3/Byers Hall, Suite 203, 1700 4th Street, University of California, San Francisco, San Francisco, CA 94158, miki.sode@ucsf.edu, Tel: 415-476-3702, Fax: 415-514-9656.

motion had greater impact on the precision of trabecular structure indices than on the densitometric indices.

The results of this study may provide a basis for establishing a threshold for motion artifacts in accordance to the study design as well as a standardized quality control protocol across operators and imaging centers.

Keywords

Motion artifacts; HR-pQCT; Sinogram; Similarity measures; Trabecular bone structure

INTRODUCTION

An increasing number of single and multi-center research and clinical studies of issues related to skeletal health have used high-resolution peripheral quantitative computed tomography (HR-pQCT) for non-invasive, *in vivo* assessment of trabecular bone structure in the peripheral skeleton. The accuracy for estimating density, cortical geometry, trabecular structure, and mechanical parameters (using micro-finite element modeling) has been validated against gold-standard measurements [1–6]. The *in vivo* reproducibility (CV_{rms}) for densitometric measures and trabecular structure indices are less than 1% and approximately 4.5%, respectively [3, 7–9]. The finite precision of these measurements can be attributed to intrinsic performance limitations of the scanner hardware and image formation process, operator-related reproducibility of the acquisition and analysis procedures, limitations of the applied image processing routines, and subject motion.

Subject motion has been, and remains, a challenge in obtaining reliable HR-pQCT scans for quantitative analysis. Repeat acquisitions are often necessary to obtain images of adequate quality. Although it takes less than 3 minutes for image acquisition during the standard *in vivo* protocol, motion artifacts are commonly observed in the reconstructed images (Figure 1), especially when imaging the forearm [3]. Subject movements during HR-pQCT image acquisition can include tremor, twitch/spasm, and gradual translations or rotations. Unlike periodic motion due to respiration, cardiac motion, blood flow, etc., these involuntary, random motions are difficult to predict and monitor.

Subject motion during image acquisition can result in severely degraded HR-pQCT image quality *in vivo*. It introduces substantial error, diminishing the accuracy and reproducibility of measurements obtained from the images. Longitudinal changes in density, cortical geometry, and trabecular structure measurements in postmenopausal women after being on anti-resorptive treatment for 12 months are at the same order of magnitude as the reproducibility [10–12]. However, individual errors can be as high as 12% and 30% with severe motion artifacts (unpublished data). Indices that describe trabecular structure are likely more prone to such errors compared to densitometric indices [3]. Because trabeculae span only 1–3 voxels in width, the depiction of the trabecular structure is subject to significant, variable partial volume averaging – a challenge for threshold-based analyses.

The detection and correction for subject motion in tomographic image data has been the subject of considerable research effort [13–18]. As three-dimensional computed tomography images are reconstructed from a series of projection images collected across 180° over a certain integration time, subject motion during acquisition modifies each projection according to its magnitude, mode, and timing. Therefore, the set of projections collected during a tomographic acquisition encode temporal and spatial information of the motion. The majority of approaches focus on an analysis of sinogram shape. The edge of an object in the projection appears sinusoidal in the sinogram space, hence the deviation from the

idealized sinusoidal line is assumed to be due to subject motion. Fiducial markers [14], or anatomical landmarks are often traced in the sinogram space.

In an effort to provide a guideline for grading image quality, the manufacturer has provided a qualitative grading system according to the apparent severity of motion artifacts in the image (Figure 1). The criteria for grading, however, are highly subjective, are not based on a quantitative measurement, and have not been related to error in bone quality outcome parameters. While this image quality grading system can distinguish the worst image quality (grade 4 or 5) from the best quality (grade 1 or 2), the discriminatory power is not linear or reliable (unpublished data).

If subject motion in the image can be quantified, the magnitude of motion-induced error in the measurements can be predicted. Such a procedure is essential for establishing not only a threshold for motion artifacts in order to control for image quality to detect the difference in accordance to the study design, but also a standardized quality control protocol across operators and imaging centers. It also allows realistic assessment and comparison across study results that use *in vivo* HR-pQCT. Therefore, an objective, standardized procedure for repeating the acquisition based on empirical data that allows immediate decision-making in a clinical setting is necessary.

The objective of this study is three-fold: (1) to develop a metric for quantifying subject motion objectively during an HR-pQCT acquisition (quantitative motion estimate, QME), and (2) to define parameter-specific relationships between the metric and expected precision error.

METHODS

1. Proposed method for an objective detection of subject motion

In this study, we propose an objective technique for measuring subject motion based on a comparison of image similarity measure of the parallelized projections acquired at 0° and 180°. Figure 2 summarizes the workflow of the proposed method for measuring the amount of motion during a single acquisition quantitatively. The proposed method is based on the assumption that if there was absolutely no motion, parallel projection images at 0° and 180° are mirror images. Any differences between these two parallel projections were, therefore, assumed to be primarily due to subject motion during the acquisition. Therefore by comparing the differences between parallel projection images at 0° and mirrored parallel projection images at 180° using a similarity measure, the subject motion can be estimated (Figure 3).

1.1 Parallelization—Divergence the cone-beam configuration of x-ray beam used in the current CT image acquisition introduces magnification that results in dissimilarity in the projections at 0° and 180° due to differences in object location with respect to the source and detector. To eliminate this magnification, a series of cone-beam projections is reformatted to a series of parallel projections (in the azimuthal/fan-beam plane). First, the dark and flat field intensities were corrected in each raw projection image. Parallel rays were collected over an interval of projections equal to the fan angle of the beam (Figure 2).

To construct a parallel projection image at an angle from the acquired raw cone-beam projection data, the beams extracted from 78 sequential projections spanning ±9.32° degrees (Figure 2), given the geometry of HR-pQCT scanner (XtremeCT, Scanco Medical, Brüttisellen, Switzerland) and acquisition protocol used in this study. The resulting parallel projection image at each angle, therefore, contained both spatial and temporal information collected over this range. A total of 3 parallel projection images at 0°, 0.24° (the second

acquired projection), and 180° were constructed from the raw cone-beam projection using the manufacturer-provided algorithm prior to the calculations of the similarity measures. The resulting images correspond to the palmar and dorsal projections for the radius, and the medial and lateral projections for the tibia (Figure 2).

The parallel projection image at 180° was then mirrored with respect to the center of rotation on the detector to match and to be compared to the parallel projection image at 0° (Figure 2). Finally, a fixed threshold was applied to the parallel projection image at 0°, to identify the region containing bone along the long axis of the detector. On average, this bone region spanned 528 pixels and 598 pixels out of 1536 pixels for the radius and tibia, respectively. The QMEs were calculated in the same region of both images.

1.2 Quantitative Motion estimates (QMEs)—The proposed motion estimate utilizes a similarity measure to compare the mirrored parallel projection image at 180° and the parallel projection image at 0°. Two similarity measures, the sum of squared intensity difference (SSD) and normalized cross correlation (NCC) were examined.

Similarity measures are metrics that assess the degree to which two images are comparable, and they have been the essential part of motion detection and image registration. These include sum or mean of squared intensity difference, cross correlation, ratio image uniformity, and mutual information. The former three measures are intensity-based methods, therefore, work better for images from the same modality as the image intensity is the same [19]. Among these measures, the sum of squared intensity difference (SSD) and normalized cross correlation (NCC) have successfully been used to compare projection images in sinogram-based motion detection [15].

Let f be the fixed image (the projection image at 0°) and g be the moving image (the projection image at 180°). The SSD and NCC are given by

$$SSD=\sum_i^N (f_i - g_i)^2, \text{ and } NCC=\frac{\sum_i^N (f_i \cdot g_i)}{\sqrt{\sum_i^N f_i^2 \cdot \sum_i^N g_i^2}},$$

where N is the number of voxels and f_i and g_i are the intensity values of the ith voxel. The greater the difference between the two images (due to motion) (Figure 3), the larger the SSD. Similarly, for NCC, the greater the difference between the two images, the larger the deviation from 1.

To account for inherent variability in bone size, density, positioning, and other covariates among subjects that may affect the magnitude of each measure, the similarity calculations were additionally performed between the projection images at 0° and the second acquired projection at 0.24°. These reference measures served as an internal control for each scan, and were assumed to reflect the subject-specific projection similarity with virtually no motion. In other words, all similarity measures between the projection images at 0° and 180° were normalized by the similarity measures between the projection images at 0° and 0.24° to account for differences bone size and density. QMEs are, therefore, dimensionless. While this ratio increases for SSD, it increasingly deviates from 1 for NCC with increased difference between the projection images at 0° and 180°. Therefore, the normalized NCC is subtracted from 1, so that the resulting QME_{NCC} increases with the degree of subject motion. Furthermore, to match the dynamic range to SSD, the motion estimate based on NCC are squared then multiplied by 100. Finally, the SSD- and NCC-based QMEs are given by:

$$QME_{SSD} = SSD_{0° \text{ vs } 180°} / SSD_{0° \text{ vs } 0.24°}, \text{ and}$$
$$QME_{NCC} = 100 \times \sqrt{(1 - NCC_{0° \text{ vs } 180°} / NCC_{0° \text{ vs } 0.24°})}.$$

Only the QMEs of the image with worse grade of a pair were included, as no a priori knowledge of the degree of motion artifact in the reconstructed image is available in a clinical setting. Motion estimate calculations were implemented using Matlab (Mathworks, Natick, MA).

2. HR-pQCT image acquisition

Subjects were imaged at least twice in a clinical HR-pQCT system (XtremeCT, Scanco Medical AG, Brüttisellen, Switzerland) using the manufacturer's standard *in vivo* protocol [3, 7, 8, 20–22]. Each subject's forearm and lower leg were positioned in the thumb-up and toe-up positions, respectively. They were then immobilized in corresponding carbon-fiber molds, and fixed to the scanner to minimize motion during acquisition. A 9.02-mm-long section (110 slices) of the radius and tibia was imaged starting at 9.5 mm and 22.5 mm proximal to the distal endplate, respectively, extending proximally. The non-dominant side was scanned unless there was a history of fracture, in which case, the contra-lateral side was scanned. The cadaveric specimens were imaged twice with repositioning in the same manner.

The x-ray source potential was 60 kVp with a current of 900 μA. A two-dimensional detector containing 3072 × 256 CCD elements was used to acquire 750 projections over 180 degrees with at a 100 ms integration time per angular position. The 12.6 cm field of view was reconstructed across a 1536 × 1536 matrix, yielding 82 μm isotropic voxels. Image acquisition time was 3 minutes per scan. Images were immediately reviewed for motion artifacts in a single low-resolution reconstructed image. Acquisition was repeated if obvious artifacts were detected. The effective dose was 3 μSv per measurement.

Attenuation values were converted to equivalent hydroxyapatite density (mg HA/cm^3) using a linear relationship based on a phantom containing cylinders of HA-resin mixtures with five different concentrations (0, 100, 200, 400, and 800 mg HA/cm^3) (QRM, Moehrendorf, Germany). For quality control, the linear attenuation values of the phantom were monitored daily.

3. HR-pQCT image analysis

The images were segmented and processed in accordance with the standard patient-style analysis protocol using Image Processing Language (Scanco Medical AG, Brüttisellen, Switzerland) as described elsewhere [3, 7, 8, 20–22]. First, a semi-automated edge-defining algorithm was applied to the original grayscale image to contour the periosteal surface. The total volumetric bone mineral density (BMD) was calculated within this contour. The cortical and trabecular regions were segmented automatically by the analysis protocol as described in detail by Laib et al [23]. Cortical and trabecular volumetric BMDs (Ct.BMD and Tb.BMD, respectively) were calculated as the mean density within the segmented corresponding volume of interest. Cortical thickness (Ct.Th) and cortical area (Ct.Ar) were calculated using an annular model approximation [24].

Calculation of the trabecular densitometric and structural indices from HR-pQCT images has been described [23], validated [2, 25, 26] and employed in a number of recent studies [3, 7–9, 20, 22, 27]. Trabecular bone volume fraction (BV/TV) is derived from Tb.BMD assuming fully mineralized bone to have 1200 mg/cc HA. From the binary image, trabecular

number (Tb.N) was obtained as the average distance between trabecular mid-axis [28, 29]. In addition, trabecular -thickness (Tb.Th), and -separation (Tb.Sp) were derived from Tb.N.

These density, cortical geometry, and trabecular structure measurements were assessed only in a common volume of interest (VOI) between two repeated measurements. The common volume of interest is identified using software provided by the manufacturer in the following manner. The periosteal cross-sectional area (CSA) was first calculated on a slice-by-slice basis for each measurement. Cross-correlation was used to determine an optimal offset between the measurements to match the CSA between scans. On average, common volume of interest between two repeated measurements accounted for 94% of a full volume acquired.

4. Image quality grading

Two trained observers independently graded all the images according to the manufacturer-suggested image quality grading system (Figure 1). Grading was based on the apparent severity of motion artifacts in the 3 slices (at the middle and both proximal and distal end slices) of the reconstructed image. In case of disagreement, a consensus grade was decided mutually.

5. Dataset

5.1 In vivo data—All datasets with repeated acquisitions of the same site acquired during a single exam collected for various studies conducted in our laboratory over the past 5 years were retrospectively evaluated. For this study, all exams with pairs that include at least one grade 1 image (no visible motion) were included. A total of 88 pairs of HR-pQCT images of the distal radius (N=54) and tibia (N=34) acquired for 49 women (age = 59 ± 14 yr) and 3 men (46 ± 2 yr) resulted. The number of pairs in each grade combination is summarized in Table 1. All subjects gave written informed consent prior to participation to each study. The protocol was approved by the University of California, San Francisco Committee on Human Research.

5.2 Specimens—To serve as the reference case without subject motion (image quality grade = 0), a total of 4 pairs of HR-pQCT images of the distal radius (N=2) and tibia (N=2) acquired for two wrists and two ankles specimens with intact hands, foot, and full surrounding soft tissues were obtained from four human donors post mortem (three males and one female, aged 74 ± 2.4 years; acquired from National Disease Research Interchange, Philadelphia, PA). Each pair contained two repeated images with repositioning.

6. Statistical Analysis

The Shapiro–Wilk W test was used to test the normality of the data. As most QMEs and the bone indices were not normally distributed, non-parametric methods were employed. First, to put it in a perspective, the variability of the QMEs was compared against the quality grade. Both the *in vivo* and specimen data were used regardless of pairing. Dunett's test was used to contrast the QMEs grouped by their qualitative grade, against the reference values obtained from the images of cadaveric specimens ("Grade 0"). To further contrast between individual grades, Wilcoxon/Kruskal-Wallis (WKW) tests and post hoc (Siegel) Tukey HSD tests were applied.

The percent difference in the cortical and trabecular densitometric, geometric, and structure indices were calculated between the images with and without motion artifact as the error introduced by the motion artifact. Regression analyses were performed to establish the relationship between the QMEs and the absolute degree of motion-induced error in the calculated bone indices from the paired analysis. Mixed-effect regression analyses were

employed, in which the subjects were treated as the random effect to account for the multiple measurements per person (e.g. multiple pairs were included for subjects with more than 2 acquisitions). The regression coefficients of the QMEs were reported. The significance was set at $\alpha = 0.05$. All statistical tests were performed using JMP (version 7.0, SAS Institute Inc., Cary, NC).

RESULTS

Variability of the QMEs with respect to image quality grade

Figure 4 displays the variability of the QMEs with respect to the image quality grade of the reconstructed HR-pQCT images at the distal radius and tibia. Both the mean values and variability (range) of the QME_{SSD} and QME_{NCC} increased proportionally with subject motion as measured by the image quality grading. Compared to that of the reference images with no motion (grade 0, from cadaveric specimens with repositioning), the mean values of QME_{SSD} were significantly higher for the images graded 3 or higher at the radius ($p < 0.05$) and 4 or higher at the tibia ($p < 0.001$) (Figure 4). Similarly, the mean values of QME_{NCC} were significantly higher for the images graded 2 and up at the radius and 3 and up at the tibia compared to that of the reference images (both $p < 0.05$) (Figure 4). Tukey HSD tests revealed that the mean values of QME_{SSD} were significantly higher for the images 3 and up, as well as 5, compared to the images with lower grade for both radius and tibia. The mean values of QME_{NCC} were not significantly different between the images with adjacent grades (e.g. 1 and 2, 2 and 3, and 3 and 4), except for between the images graded 4 and 5.

Relationship between the QMEs and the error in the indices

Mixed-effect regression analyses revealed significant associations between the degree of errors in all of the calculated indices and the QMEs (Table 2). The coefficients for the trabecular structure indices were larger than for the densitometric and cortical geometry indices for both estimates. For instance, to put it in a context, for every unit of increase in QME_{SSD}, the error increases by 0.5% and 0.2% in Tb.BMD, 0.3% and 0.5% in Ct.Th, but 1.2 and 1.5% in Tb.N at the distal radius and tibia, respectively. Similarly, for every unit of increase in QME_{NCC}, the error increases by 1.4% and 0.6% in Tb.BMD, 1.0% in Ct.Th, but 3.7% and 4.9% in Tb.N at the distal radius and tibia, respectively.

DISCUSSION

In this study, we proposed an objective, standardized procedure for repeating the HRpQCT acquisition using a quantitative motion estimate (QME), where the parallelized projection images at 0° and 180° were compared using a similarity measure. Figure 4 exhibits the overlapping ranges of QMEs between adjacent image quality grades, particularly among image grade 0 to 2, and 3 and 4. This highlights the subjective nature of the quality grading system and need for a quantitative estimate technique for measuring subject motion as proposed in this study. Both QMEs were significantly and strongly related to the motion-induced errors in the density, cortical geometry, and trabecular structure indices and their empirical relationship was laid out.

Two similarity measures, SSD and NCC, were examined for the use in the proposed procedure. Both SSD- and NCC-based QMEs (QME_{SSD} and QME_{NCC}, respectively) increased proportionally with image quality grade as assessed by two trained observers. The image quality grades were differentiated between grade 2 and 3 using QME_{SSD}, but not with QME_{NCC}, in addition to between grade 4 and 5 (Figure 4). This may be attributed to SSD being robust against the object shape, the geometry of the CT system, and beam hardening effects as found in the sinogram-based motion detection [15]. NCC is most suitable for

detecting small affine translation; however, it is less sensitive to a large translation [30, 31] as well as with noisy images as the peak of correlation may be skewed by a local maximum [32]. The performance of QME_{NCC}, therefore, may be improved by removing noise with a low-pass filter.

As measured by the proposed QME, image quality degradation due to subject motion had a greater impact on the precision of trabecular structure indices than on the densitometric indices. This is consistent with generally poorer *in vivo* reproducibility of micro-structural measures reported by a number of groups [3, 7–9]. The mean percent age-related difference in Tb.BMD, Ct.Th, and Tb.N at the distal radius in women are approximately −3.2%, −5.2% and −3.2% per decade, respectively [33, 34]. For Tb.BMD and Ct.Th, such degree of error is expected from the images with QME_{SSD} = 2.6 and 3.8, and QME_{NCC} = 7.4 and 19, respectively, which corresponds to upper bound of the images with quality grade 3 score or higher; For Tb.N, however, a 3.2% of error can be achieved with QME_{SSD} = 1 and $QME_{NCC} < 0$, therefore, no subject tolerated. Similarly, the mean differences in Tb.BMD, Ct.Th, and Tb.N at the distal radius between premenopausal women and postmenopausal osteopenic and/or osteoporotic women are up to −36.7%, −39.4% and −22.7% [7, 35]. While QME associated with such degree of difference in Tb.BMD and Ct.Th is beyond the range observed in this study, QME_{SSD} = 3.8 and QME_{NCC} = 14.8 is enough to introduce 22.7% error in Tb.N, which is within the range for image graded 5 (Figure 4).

The strength of the proposed approach for detecting subject movement during HR-pQCT image acquisition is that it is quantitative (objective) and implementable for a clinical use. Since the proposed method is objective approach to quantify subject motion, a decision for repeating the acquisition can be standardized across operator, scanner, and sites for a large-scale study. The use of raw projections for the motion detection process allows an immediate response in case a motion artifact is suspected without waiting for the reconstruction process to complete. The clear definition of the acceptance/rejection criteria saves the subject from unnecessary radiation exposure.

The empirical relationship between the QMEs and the errors in the calculated indices reported in this study can be a basis for establishing a threshold in which to accept or reject an image or to include or exclude a measurement that fits the specific study design. For instance, if a study objective is to detect a 5% difference in a densitometric or cortical index, a threshold for motion artifact can be set at QME_{SSD} = 3 and QME_{NCC} = 11, based on % ΔTb.BMD at the distal radius (Table 2). According to Figure 4, they are approximately at the upper bound of the typical range of the respective motion estimate for the images with grade 4 motion artifacts. However, if a study objective is to detect a 5% difference in Tb.N, a threshold is at 1.2 and 0, respectively. Therefore, no subject motion can be tolerated.

There are several technical limitations inherent to the proposed method worth noting. The fact that the HR-pQCT image acquisition process does not cover a full 360° means that only 0° image and the mirrored 180° images can be compared. Although temporal and spatial information are contained in the 78 sequential cone-beam projections that are utilized to construct the parallelized 0° image and 180° projections, this accounts for just 20% of the entire acquired time (Figure 2). The information contained in the remaining 80% is not fully utilized. For instance, if the arm or leg twitched and came back to the exact same spatial location within this interval, it will be undetected when comparing 0° and 180° images; yet the reconstructed images will still exhibit motion-degradation.

Furthermore, motion estimates based on a similarity measure between the first and last projections as well as image quality grading system likely have variable sensitivity to magnitude and different modes of motion. First, the magnitude has to be large enough to

cause a detectable difference between 180° image and 0° image. Second, it is reasonable to expect that the proposed method is more sensitive to permanent translation parallel to the detector plane. Conversely, it is less sensitive to translation perpendicular to the detector plane. Their relative sensitivity for other modes of subject movement, such as rotational displacement, however, is not clear. Therefore, the correlation between the degree of error in the index of interest and the magnitude and mode of motion must also be elucidated. A future study should evaluate the sensitivity of the proposed method in detecting both rotational and translational movements in a controlled manner.

In conclusion, an objective technique for measuring subject motion during HR-pQCT image acquisition has been proposed, in which the parallelized projection images at 0° and 180° were compared using a similarity measure. This study is an attempt to quantify the subject movement during HR-pQCT image acquisition *in vivo*, as well as to quantify the impact of such motion on trabecular structure indices. The results of this study may provide a basis for establishing a threshold for motion artifacts in accordance to the study design. Consequently, a quality control protocol for providing the operator with immediate feedback on image quality and for post hoc inclusion/exclusion quality control can be standardized. Ultimately such practice will results in allowing realistic interpretation and comparison across study results that was assessed using *in vivo* HR-pQCT.

References

1. Liu XS, Zhang XH, Sekhon KK, Adam MF, McMahon DJ, Bilezikian JP, Shane E, Guo XE. High-Resolution Peripheral Quantitative Computed Tomography Can Assess Microstructural and Mechanical Properties of Human Distal Tibial Bone. J Bone Miner Res. 2010; 25:746–56. [PubMed: 19775199]
2. MacNeil JA, Boyd SK. Accuracy of high-resolution peripheral quantitative computed tomography for measurement of bone quality. Med Eng Phys. 2007; 29:1096–105. [PubMed: 17229586]
3. MacNeil JA, Boyd SK. Improved reproducibility of high-resolution peripheral quantitative computed tomography for measurement of bone quality. Med Eng Phys. 2008; 30:792–9. [PubMed: 18164643]
4. Sekhon K, Kazakia GJ, Burghardt AJ, Hermannsson B, Majumdar S. Accuracy of volumetric bone mineral density measurement in high-resolution peripheral quantitative computed tomography. Bone. 2009; 45:473–9. [PubMed: 19501201]
5. Sode M, Burghardt AJ, Nissenson RA, Majumdar S. Resolution dependence of the non-metric trabecular structure indices. Bone. 2008; 42:728–36. [PubMed: 18276202]
6. Varga P, Zysset PK. Assessment of volume fraction and fabric in the distal radius using HR-pQCT. Bone. 2009; 45:909–17. [PubMed: 19615478]
7. Boutroy S, Bouxsein ML, Munoz F, Delmas PD. In vivo assessment of trabecular bone microarchitecture by high-resolution peripheral quantitative computed tomography. J Clin Endocrinol Metab. 2005; 90:6508–15. [PubMed: 16189253]
8. Kazakia GJ, Hyun B, Burghardt AJ, Krug R, Newitt DC, de Papp AE, Link TM, Majumdar S. In vivo determination of bone structure in postmenopausal women: a comparison of HR-pQCT and high-field MR imaging. J Bone Miner Res. 2008; 23:463–74. [PubMed: 18052756]
9. Khosla S, Riggs BL, Atkinson EJ, Oberg AL, McDaniel LJ, Holets M, Peterson JM, Melton LJ 3rd. Effects of sex and age on bone microstructure at the ultradistal radius: a population-based noninvasive in vivo assessment. J Bone Miner Res. 2006; 21:124–31. [PubMed: 16355281]
10. Burghardt AJ, Kazakia GJ, Sode M, de Papp AE, Link TM, Majumdar S. A longitudinal HR-pQCT study of alendronate treatment in post-menopausal women with low bone density: Relations between density, cortical and trabecular micro-architecture, biomechanics, and bone turnover. J Bone Miner Res. 2010; 25:2282–95.
11. Rizzoli R, Laroche M, Krieg MA, Frieling I, Thomas T, Delmas P, Felsenberg D. Strontium ranelate and alendronate have differing effects on distal tibia bone microstructure in women with osteoporosis. Rheumatol Int. 30:1341–8. [PubMed: 20512336]

12. Seeman E, Delmas PD, Hanley DA, Sellmeyer D, Cheung AM, Shane E, Kearns A, Thomas T, Boyd SK, Boutroy S, Bogado C, Majumdar S, Fan M, Libanati C, Zanchetta J. Microarchitectural deterioration of cortical and trabecular bone: Differing effects of denosumab and alendronate. J Bone Miner Res. 2010; 25:1886–94. [PubMed: 20222106]

13. Pauchard, Y.; Ayres, FJ.; Boyd, SK. Measuring patient motion in HR-pQCT. In: Biomedical Imaging: From Nano to Macro, 2009. ISBI '09. IEEE International Symposium on; 2009. p. 338-341.

14. Pauchard, Y.; Boyd, SK. Landmark based compensation of patient motion artifacts in computed tomography. Jiang, H.; Ehsan, S., editors. SPIE; -2008.p. 69133C

15. Ens, S.; Muller, J.; Kratz, B.; Buzug, TM. Sinogram-Based Motion Detection in Transmission Computed Tomography. In: Magjarevic, R., editor. 4th European Conference of the International Federation for Medical and Biological Engineering; Berlin Heidelberg: Springer; 2009. p. 505-508.

16. Yu H, Wang G. Data consistency based rigid motion artifact reduction in fan-beam CT. IEEE Trans Med Imaging. 2007; 26:249–60. [PubMed: 17304738]

17. Lu W, Mackie TR. Tomographic motion detection and correction directly in sinogram space. Phys Med Biol. 2002; 47:1267–84. [PubMed: 12030555]

18. Zerfowski, D. Motion Artifact Compensation in CT. Proceedings - SPIE The International Society for Optical Engineering; 1998. p. 416-425.

19. Hajnal JV, Saeed N, Soar EJ, Oatridge A, Young IR, Bydder GM. A Registration and Interpolation Procedure for Subvoxel Matching of Serially Acquired MR Images. Journal of Computer Assisted Tomography. 1995; 19:289–296. [PubMed: 7890857]

20. Dalzell N, Kaptoge S, Morris N, Berthier A, Koller B, Braak L, van Rietbergen B, Reeve J. Bone micro-architecture and determinants of strength in the radius and tibia: age-related changes in a population-based study of normal adults measured with high-resolution pQCT. Osteoporos Int. 2009; 20:1683–94. [PubMed: 19152051]

21. Melton LJ 3rd, Riggs BL, van Lenthe GH, Achenbach SJ, Muller R, Bouxsein ML, Amin S, Atkinson EJ, Khosla S. Contribution of in vivo structural measurements and load/strength ratios to the determination of forearm fracture risk in postmenopausal women. J Bone Miner Res. 2007; 22:1442–8. [PubMed: 17539738]

22. Vico L, Zouch M, Amirouche A, Frère D, Laroche N, Koller B, Laib A, Thomas T, Alexandre C. High-Resolution pQCT Analysis at the Distal Radius and Tibia Discriminates Patients With Recent Wrist and Femoral Neck Fractures. Journal of Bone and Mineral Research. 2008; 23:1741–1750. [PubMed: 18665795]

23. Laib A, Hauselmann HJ, Ruegsegger P. In vivo high resolution 3D-QCT of the human forearm. Technol Health Care. 1998; 6:329–37. [PubMed: 10100936]

24. Davis KA, Burghardt AJ, Link TM, Majumdar S. The effects of geometric and threshold definitions on cortical bone metrics assessed by in vivo high-resolution peripheral quantitative computed tomography. Calcif Tissue Int. 2007; 81:364–71. [PubMed: 17952361]

25. Laib A, Ruegsegger P. Calibration of trabecular bone structure measurements of in vivo three-dimensional peripheral quantitative computed tomography with 28-microm-resolution microcomputed tomography. Bone. 1999; 24:35–9. [PubMed: 9916782]

26. Muller R, Hildebrand T, Hauselmann HJ, Ruegsegger P. In vivo reproducibility of three-dimensional structural properties of noninvasive bone biopsies using 3D-pQCT. J Bone Miner Res. 1996; 11:1745–50. [PubMed: 8915782]

27. Sornay-Rendu E, Boutroy S, Munoz F, Delmas PD. Alterations of cortical and trabecular architecture are associated with fractures in postmenopausal women, partially independent of decreased BMD measured by DXA: the OFELY study. J Bone Miner Res. 2007; 22:425–33. [PubMed: 17181395]

28. Laib A, Hildebrand T, Hauselmann HJ, Ruegsegger P. Ridge number density: a new parameter for in vivo bone structure analysis. Bone. 1997; 21:541–6. [PubMed: 9430245]

29. Mueller TL, Stauber M, Kohler T, Eckstein F, Muller R, van Lenthe GH. Non-invasive bone competence analysis by high-resolution pQCT: an in vitro reproducibility study on structural and mechanical properties at the human radius. Bone. 2009; 44:364–71. [PubMed: 19027092]

30. Maes F, Vandermeulen D, Suetens P. Medical image registration using mutual information. Proceedings of the IEEE. 2003; 91:1699–1722.

31. Tsai D-M, LIN C-T. Fast normalized cross correlation for defect detection. Pattern Recognition Letters. 2003; 24:2625–2631.

32. Brown L. A survey of image registration techniques. ACM Comput Surv. 1992; 24:325–376.

33. Macdonald HM, Nishiyama KK, Kang J, Hanley DA, Boyd SK. Age-related patterns of trabecular and cortical bone loss differ between sexes and skeletal sites: A population-based HR-pQCT study. J Bone Miner Res. 2010; 26:50–62. [PubMed: 20593413]

34. Sode M, Burghardt AJ, Kazakia GJ, Link TM, Majumdar S. Regional variations of gender-specific and age-related differences in trabecular bone structure of the distal radius and tibia. Bone. 2010; 46:1652–60. [PubMed: 20188877]

35. Nishiyama KK, Macdonald HM, Buie HR, Hanley DA, Boyd SK. Postmenopausal women with osteopenia have higher cortical porosity and thinner cortices at the distal radius and tibia than women with normal aBMD: an in vivo HR-pQCT study. J Bone Miner Res. 2010; 25:882–90. [PubMed: 19839766]

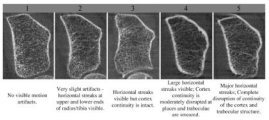

Figure 1.
Image quality grading guideline suggested by the manufacturer and representative reconstructed grayscale image of the distal radius for each grade.

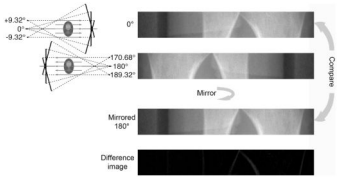

Figure 2.

Schematic drawing explaining the analysis process. Two parallelized projection images at 0° and at 180° are each reformatted from a continuous sequence of 78 cone-beam projections. The 180° projection was mirrored and compared to the 0° projection to calculate SSD and NCC-based estimates of motion (QME_{SSD} and QME_{NCC}, respectively). For the ideal case where there is no motion, the difference image between the two parallelized projection images should be zero.

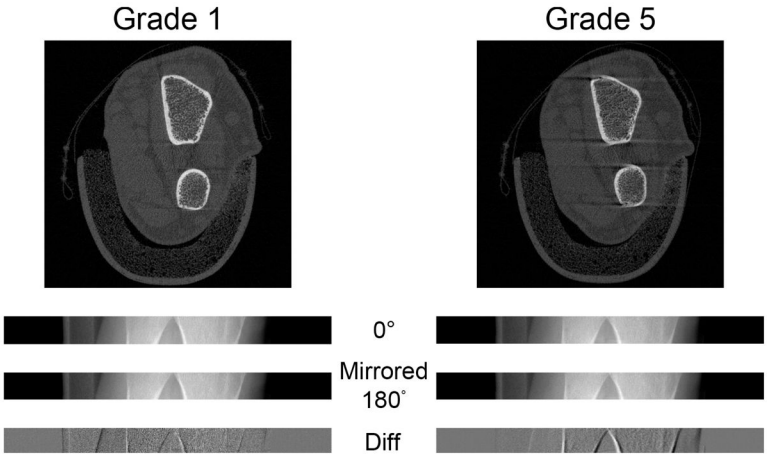

Figure 3.
Comparison of radius scans from a subject with a grade 1 score (left) and a grade 5 score (right). From the top: the reconstructed images, parallelized projection images at 0°, flipped parallelized projection images at 180°, and the difference images of the two. For grade 5, the flipped parallelized projection image at 180° is shifted to the right with respect to the parallelized projection image at 0°. This offset is also apparent in the difference image with more defined edges of the projected bone contour

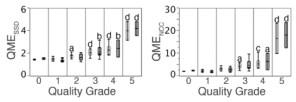

Figure 4.
Variability of the QMEs with respect to the image quality grade of the reconstructed HR-pQCT images at the distal radius (gray) and tibia (black). $^{a}p < 0.05$; $^{b}p < 0.01$; $^{c}p < 0.001$; $^{d}p < 0.0001$ with respect to the quality grade 0 (cadaveric specimens with repositioning) determined by the Dunett's test.

Table 1

Number of samples in each grade pair.

Pairs	N		
	Total	N Radius	Tibia
1-1	14	4	10
1–2	23	16	7
1–3	36	24	12
1–4	11	8	3
1–5	4	2	2
TOTAL	88	54	34

Table 2

The mixed effect regression coefficients for QME_{SSD} and QME_{NCC} and the motion-induced absolute percent errors in the densitometric, cortical geometric and trabecular structure indices at the distal radius and tibia.

QME_{SSD}	%Δ Tot.BMD		%Δ Ct.BMD		%Δ Tb.BMD		%Δ Ct.Th		%ΔCt.Ar		%Δ BV/TV		%Δ Tb.N		%Δ Tb.Th		%Δ Tb.Sp	
	Rad	Tib	Rad	Tib	Rad	Tib	Rad	Tib	Rad	Tib	Rad	Tib	Rad	Tib	Rad	Tib	Rad	Tib
Intercept	0.1	0.4	-1.5^{d}	-0.7^{a}	-3.9^{d}	−1.1	-2.0^{b}	-2.7^{b}	−0.7	-2.0^{a}	-3.8^{d}	-1.1^{a}	−4.0	−5.9	1.3	−2.3	−2.8	−3.7
Slope	0.3	0.1	1.2^{d}	0.9^{d}	2.7^{d}	1.2^{d}	1.9^{d}	2.2^{d}	1.1^{c}	1.8^{c}	2.7^{d}	1.2^{d}	7.0^{d}	8.8^{d}	3.3^{b}	5.6^{c}	5.8^{d}	6.7^{d}

QME_{NCC}	%Δ Tot.BMD		%Δ Ct.BMD		%Δ Tb.BMD		%Δ Ct.Th		%ΔCt.Ar		%Δ BV/TV		%Δ Tb.N		%Δ Tb.Th		%Δ Tb.Sp	
	Rad	Tib	Rad	Tib	Rad	Tib	Rad	Tib	Rad	Tib	Rad	Tib	Rad	Tib	Rad	Tib	Rad	Tib
Intercept	0.5^{a}	0.5^{b}	0.0	0.2	−0.5	0.1	−0.5	−0.4	0.7^{b}	−0.3	−0.5	0.1	5.0^{c}	4.6^{a}	5.6^{d}	4.6^{b}	4.8^{d}	4.5^{a}
Slope	0.1	0.0	0.2^{d}	0.2^{d}	0.5^{d}	0.2^{d}	0.3^{d}	0.4^{d}	0.1^{c}	0.4^{c}	0.5^{d}	0.2^{d}	1.2^{d}	1.5^{c}	0.5^{b}	0.9^{b}	1.0^{d}	1.1^{c}

[a] N.B. $p < 0.05$;

[b] $p < 0.01$;

[c] $p < 0.001$;

[d] $p < 0.0001$.